OPTIMAL INCREMENTAL APPROXIMATION FOR THE ADAPTIVE SOLUTION OF DIFFERENTIAL EQUATIONS

Andrew J. Meade Jr.*, Michael Kokkolaras, and Boris A. Zeldin
Department of Mechanical Engineering and Materials Science
William Marsh Rice University
6100 Main St., Houston, Texas, 77005-1892, USA
Phone: (713) 737-5880
FAX: (713) 285-5423
E-mail: meade@rice.edu

Submitted to *International Journal for Numerical Methods in Engineering*

---

* Recipient of correspondence.
This work was supported under NASA grant number CRA2-35504 and ONR grant N00014-95-1-0741.

OPTIMAL INCREMENTAL APPROXIMATION FOR THE ADAPTIVE SOLUTION OF DIFFERENTIAL EQUATIONS

Andrew J. Meade, Jr.*, Michael Kokkolaras†, and Boris A. Zeldin‡
Department of Mechanical Engineering and Materials Science,
William Marsh Rice University
6100 Main St., Houston, TX 77005-1892, USA

Key Words: Incremental approximation, basis functions, variational principles, adaptivity, optimization, parallel direct search.

Abstract

A method for optimal incremental function approximation is proposed for the solution of differential equations. The basis functions and associated coefficients of a series expansion, representing the solution, are optimally selected at each step of the algorithm according to appropriate error minimization criteria; the solution is built sequentially. In this manner, the computational technique is adaptive in nature, although a grid is neither built nor adapted in the traditional sense using a-posteriori error estimates. Variational principles are utilized for the definition of the objective function to be extremized in the associated optimization problems, ensuring that the problems are well-posed. Complicated data structures, expensive remeshing algorithms, and systems solvers are avoided. Computational efficiency is increased by using low-order basis functions and the parallel direct search optimization technique. Numerical results and convergence rates are reported for linear nonself-adjoint and nonlinear problems associated with general boundary conditions. Generalization aspects of the method are discussed.

*Associate Professor. Recipient of correspondence, e-mail: meade@rice.edu.
†Research Associate.
‡Currently with Parametric Technology Corporation.

OPTIMAL INCREMENTAL APPROXIMATION FOR THE ADAPTIVE SOLUTION OF DIFFERENTIAL EQUATIONS

Andrew J. Meade, Jr.[§], Michael Kokkolaras[¶], and Boris A. Zeldin[‖]
Department of Mechanical Engineering and Materials Science,
William Marsh Rice University
6100 Main St., Houston, TX 77005-1892, USA

1 Introduction

A method of optimal incremental approximation for the adaptive solution of differential equations is proposed. The presented method is based on concepts borrowed from the fields of artificial neural network modelling and adaptive grid optimization. The mathematical formulation of the proposed algorithm has been presented in reference [1] in conjunction with one- and two-dimensional boundary value problems involving linear, self-adjoint differential operators and homogeneous Dirichlet boundary conditions. In this paper, the proposed method will be applied to linear nonself-adjoint and nonlinear problems with general boundary conditions. The efficient adaptive nature of the computational technique will be illustrated by means of numerical results.

The paper is organized as follows. Section 2 contains a brief review of adaptive grid optimization, which motivated the development of the proposed method presented in Section 3. The optimal incremental approximation algorithm is applied to a linear nonself-adjoint problem in Section 4 and a nonlinear problem in Section 5, where the one-dimensional convection-diffusion equation and the two-dimensional velocity potential equation govern-

[§]Associate Professor. Recipient of correspondence, e-mail: meade@rice.edu.
[¶]Research Associate.
[‖]Currently with Parametric Technology Corporation.

ing compressible, irrotational and isentropic fluid flow are considered, respectively. Generalization issues will be addressed in Section 6 and conclusions will be drawn in Section 7.

2 Adaptive grids and optimization

Optimization in computational mechanics has typically focused on the grid selection in order to minimize the associated discretization error. One approach is to define some function, e.g. a nodal density function or a system energy function, as a criterion for optimal node distribution [2, 3, 4, 5]. This criterion can then be utilized as the objective function in an appropriate optimization problem for the relocation of the nodes. Unfortunately, this approach can be impractical due to the complexity and high dimensionality of the associated optimization problem; numerical results were reported only for extremely coarse grids. Moreover, derivatives, essential for gradient-based optimization techniques, can be either computationally expensive or unavailable. In addition, the application of this approach is limited to problems governed by self-adjoint, positive definite differential operators.

Modern adaptive techniques are based on the homogeneous distribution of the local approximation error, e.g. over the elements in a finite element method [6, 7, 8]. A grid is generated and a solution is found. The grid is then adapted and regenerated according to a-posteriori error estimates. The user can choose between the h-, p-, and r- methods, as they are popularly known, and their possible combinations. Multigrid methods also share this a-posteriori error estimation and adaptation philosophy.

It is well-known that most of the computational time required by codes that utilize adaptive or multigrid techniques is spent on the necessary grid generation. According to Oden [9], the major challenges of adaptive methods in computational fluid dynamics include, 1) the use of unstructured meshes and therefore elaborate and complicated data structures, 2) the necessity of explicit or iterative solution techniques due to the poor performance of direct solvers on dynamically evolving unstructured meshes, 3) stability issues of the associated numerical schemes stemming from the continuous changes in the orders and structures, and 4) the computational overhead of the error estimation and the adaptation process.

The method presented in this paper features the advantages of adaptive methods without sharing their disadvantages. Specifically, while the method is adaptive in an iterative manner and is based on the optimization of some appropriate criterion, the dimensionality of the associated optimization problem is kept low, derivatives are not required, and most importantly, a grid is not built in the traditional sense. Unstructured mesh data structures are not required for the realization of the method due to the use of simple tensor products of low-order basis functions. Moreover, computationally expensive matrix-assembling algorithms and solvers of systems of equations are avoided. Variational principles and weighted residuals concepts are utilized to define well-posed optimization problems; numerical stability issues are limited to the nonlinear optimization process. Most significantly, the "grid", defined by the location of the optimally selected basis functions, evolves with the solution and is not based on a-posteriori error estimates; the computational overhead of the a-posteriori error estimation and respective regridding is eliminated due to a sequential error estimation and adaptation process.

3 The proposed method

The proposed algorithm for optimal incremental approximation has been based on the artificial neural network algorithm proposed by Jones [10, 11] and Barron [12].

The solution $u(\bar{x})$ of a problem is approximated by the series expansion

$$u(\bar{x}) \approx u_N^a(\bar{x}) = u_0 + \sum_{j=1}^{N} c_j \Phi_j(\bar{x}, \bar{p}_j) \ , \tag{1}$$

where u_0 is some initial approximation, typically present for the satisfaction of nonhomogeneous Dirichlet boundary conditions. The expansion coefficients and basis functions are represented by c_j and Φ_j, respectively. At a stage of the algorithm N, the parameters $\bar{p}_N$ of the function Φ_N and the associated coefficient c_N are optimally selected according to an appropriate criterion, i.e. by solving a nonlinear optimization problem, while holding c_j and $\Phi_j(\bar{x}, \bar{p}_j)$ fixed for $j = 1, \ldots, N-1$.

Variational principles are utilized to define the objective function of the well-posed low-dimensional optimization problem which is then solved by means of the efficient parallel direct search (PDS) optimization technique [13]. PDS is a collection Fortran routines for solving both unconstrained and constrained nonlinear optimization problems using direct search methods. Direct search methods have the advantage of requiring information about the objective function only; derivatives do not need to be calculated. Moreover, the necessary function evaluations can be performed in parallel by means of the message passing interface (MPI). Scalability is achieved by fully exploiting additional processors. The search size is controlled by the user.

4 Linear problems

The application of the proposed method of optimal incremental approximation was demonstrated in reference [1] for linear self-adjoint problems with homogeneous Dirichlet boundary conditions. In this section, a linear nonself-adjoint problem with nonhomogeneous Dirichlet boundary conditions will be considered.

A mathematical model of adequate fidelity for the steady-state balance between fluid convection and diffusion is given by the following differential equation

$$-\alpha \frac{d^2 u}{dx^2} + \beta \frac{du}{dx} = 0 \quad \text{with} \quad \alpha, \beta > 0 \;, \quad 0 \leq x \leq 1 \;, \tag{2}$$

where α and β represent the viscosity and convection coefficients, respectively. Equation (2) is nondimensionalized and, in combination with the nonhomogeneous Dirichlet boundary conditions $u(0) = 0$ and $u(1) = 1$, possesses the exact solution

$$u(x) = \frac{e^{\frac{\beta}{\alpha}x} - 1}{e^{\frac{\beta}{\alpha}} - 1} \;. \tag{3}$$

The solution function u, representing velocity, is characterized by the presence of a boundary layer adjacent to the boundary at $x = 1$ [14]. From a physical perspective, dissipation is for many flow problems of significance only in the region of the boundary layer. Therefore, numerical solutions are often oscillatory when the dependent variable exhibits large gradients across the boundary layer. In finite difference methods for example, the so-called cell Reynolds number, defined in analogy to the freestream Reynolds number by $Re_{cell} = \frac{\beta \Delta x}{\alpha}$, plays a significant role in the accuracy and oscillations of the numerical solution. Equation (2) poses, in this regard, a challenging numerical problem.

A linear nonself-adjoint differential operator $L[\cdot]$ may be transformed to a self-adjoint operator $L^{'}[\cdot]$ if some appropriate function P exists such that $L^{'}[\cdot] = P(x)L[\cdot]$ [15]. For the example considered, $P(x) = e^{-\frac{\beta}{\alpha}x}$ (see Appendix A). Given the linear, self-adjoint differential operator $L^{'}[\cdot] = P(x)L[\cdot]$, the variational principle associated with Equation (2) is defined as

$$E \equiv \frac{1}{2}\langle u, L^{'}[u]\rangle \ , \tag{4}$$

provided that the boundary conditions are homogeneous. The inner product $\langle\cdot,\cdot\rangle$ is defined as $\langle w, z\rangle = \int_\Omega wz d\bar{x}$. After adjusting the variational principle to account for nonhomogeneous boundary conditions [16], integrating by parts, and omitting terms that are independent of u, the final variational integral reads as

$$E = \int_0^1 e^{-\frac{\beta}{\alpha}x} \left(\frac{du}{dx}\right)^2 dx \ . \tag{5}$$

4.1 Numerical procedure

The function $u(x)$ that minimizes the functional in Equation (5) satisfies the associated Euler-Lagrange equation (Equation (2)) with boundary conditions. The series expansion used for the approximation of $u(x)$ is

$$u(x) \approx u_N^a(x) = x + \sum_{j=1}^{N} c_j \Phi_j(x, \bar{p}_j) = u_{N-1}^a(x) + c_N \Phi_N(x, \bar{p}_N) \ , \tag{6}$$

where the term $c_0\Phi_0 = x$ is included in order to satisfy the boundary conditions, since all of the functions Φ_j, $j = 1, \ldots, N$ are restricted to vanish at the boundaries. By introducing this series expansion into Equation (5), the augmented optimization variables vector $\bar{p}_N^{'} =$

$(\bar{p}_N, c_N)^{\mathrm{T}}$ can be determined using PDS. The size of this nonlinear optimization problem can be reduced; after substituting Equation (6) into Equation (5), differentiating E with respect to c_N and equating the result to zero, the following expression is obtained

$$\int_0^1 e^{-\frac{\beta}{\alpha}x} \frac{du_N^a}{dx} \frac{d\Phi_N}{dx} dx = 0 \ . \tag{7}$$

Solving for the coefficient c_N yields

$$c_N = \left[\int_0^1 e^{-\frac{\beta}{\alpha}x} \frac{d\Phi_N}{dx} \frac{d\Phi_N}{dx} dx \right]^{-1} \left[- \int_0^1 e^{-\frac{\beta}{\alpha}x} \frac{d\Phi_N}{dx} dx - \sum_{j=1}^{N-1} c_j \int_0^1 e^{-\frac{\beta}{\alpha}x} \frac{d\Phi_j}{dx} \frac{d\Phi_N}{dx} dx \right] \ . \tag{8}$$

The parameters $\bar{p}_N$ of the N-th basis function can now be computed by minimizing the functional

$$E(u_N^a) = \int_0^1 e^{-\frac{\beta}{\alpha}x} \left(1 + \sum_{j=1}^{N-1} c_j \frac{d\Phi_j}{dx} + \left[\int_0^1 e^{-\frac{\beta}{\alpha}x} \frac{d\Phi_N}{dx} \frac{d\Phi_N}{dx} dx \right]^{-1} \times \right.$$
$$\left. \left[- \int_0^1 e^{-\frac{\beta}{\alpha}x} \frac{d\Phi_N}{dx} dx - \sum_{j=1}^{N-1} c_j \int_0^1 e^{-\frac{\beta}{\alpha}x} \frac{d\Phi_j}{dx} \frac{d\Phi_N}{dx} dx \right] \frac{d\Phi_N}{dx} \right)^2 dx \ , \tag{9}$$

while the associated coefficient c_N can be determined from Equation (8).

Readily parameterized, piecewise linear, "hat" (B_1-splines) functions are employed to ensure computational efficiency. B_1-splines are defined as

$$\Phi(x) = \begin{cases} \frac{x-(x_M-\Delta x_l)}{\Delta x_l} & \text{if} \quad x_M - \Delta x_l \leq x \leq x_M \\ \frac{(x_M+\Delta x_r)-x}{\Delta x_r} & \text{if} \quad x_M \leq x \leq x_M + \Delta x_r \\ 0 & \text{otherwise} \end{cases} \ , \tag{10}$$

where the parameters x_M, Δx_l, and Δx_r denote the location of the center of the function, its width to the left, and its width to the right, respectively. In this regard, the optimization variables vector is given by $\bar{p}_N = (x_M, \Delta x_l, \Delta x_r)^{\mathrm{T}}$.

4.2 Numerical results

The approximate solution obtained after optimally selecting 14 basis functions, and associated coefficients, are compared to the exact solution in Figure 1 for $\frac{\beta}{\alpha} = 20$. There is satisfactory agreement between the exact and approximate solutions within the boundary layer characterized by the large gradient. The relatively low number of basis functions necessary, when compared to the uniform grid solution, confirm the potential of the method.

Fletcher presents two plots in reference [14] in order to illustrate the oscillations in solutions obtained by the finite difference method. The same kind of oscillations occur when applying the Bubnov-Galerkin finite element method to the original differential equation using coarse uniform grids and linear Lagrangian shape functions, as can be seen in Figure 2. In contrast, the solutions obtained at the early stages of the proposed method for optimal incremental approximation, presented in Figure 3, do not exhibit any oscillations and achieve higher accuracy levels. It is interesting to note that applying the Bubnov-Galerkin method to the modified differential equation is equivalent to applying the Petrov-Galerkin method to the original problem with the weighting function defined as $\Psi = e^{-\frac{\beta}{\alpha}x}\Phi$, where Φ is the shape function. In this manner, the oscillations in the obtained solutions are eliminated. However, the convergence rate is not improved.

Figure 4 compares the RMS error convergence rate obtained by the Galerkin methods using linear Lagrangian shape functions on a uniform grid to that obtained by the optimal incremental approximation method. The RMS error was calculated based on 101 uniformly distributed trial points. Since the RMS error is related to the discrete L_2-norm of the error by the following expression

$$\mathrm{RMS}_M = \sqrt{\frac{|| \ u_{ex} - u_N^a \ ||_{L_2}^2}{M}} \ , \tag{11}$$

where M is the number of trial points, and noting that the square of the discrete L_2-norm of the error is proportional to the grid spacing, then we can relate the L_2-norm of the error to the number of linear Lagrangian shape functions

$$|| \ u_{ex} - u_N^a \ ||_{L_2}^2 = Ch^2 = \frac{C}{(N-1)^2} \ , \quad C > 0 \ . \tag{12}$$

Figure 4 shows that the constant C is substantially reduced by the proposed method; in addition, the convergence rate is locally superquadratic.

Figure 5 illustrates the adaptive nature of the proposed method. Specifically, the first

10 optimally selected basis functions are plotted. It is clear that the basis functions are concentrated in the region of the large gradient.

4.3 Computational cost

The search size and the associated requisite computational cost are affected by two user-controlled parameters, the number of simplex vertices d and a tolerance tol. PDS evaluates the objective function at d vertices of a simplex in the hyperplane of dimension n, where n is the number of optimization variables. After the completion of this process, the "best" vertex is chosen and compared to the previous iterate. If the difference lies between the user-defined tolerance tol, the PDS algorithm is terminated, otherwise, a new PDS internal iteration is performed with the current iterate as the initial guess. For constrained problems, m is restricted by the condition $m \geq n^2 + n$. However, a larger m than required should be used in order to guarantee a fine search. In general, a small d should be associated with a tight tolerance tol, while a large d should be combined with a relaxed tolerance tol.

Table 1 summarizes the amount of computational work required by PDS for the example problem with $tol = 10^{-6}$ and 10^{-4}. The number of iterations required and the number of function and constraint evaluations do not fluctuate significantly. As expected, a low number of pattern points associated with a tighter tolerance requires more iterations but fewer function and constraint evaluations than a large number of pattern points associated with a relaxed tolerance. Note that for the two values of tol the algorithm requires less work in its initial stage than in all the subsequent steps.

5 Nonlinear problems

The derivation of natural variational principles for problems that are governed by nonlinear differential operators is generally a challenging task. However, there are applications of interest in fluid dynamics for which variational integrals have been proposed [17, 18, 19]. For example, the problem of compressible inviscid fluid flow has been studied in its variational form extensively. Prozan discusses the existence of variational principles for unsteady conditions in one and two dimensions in references [20] and [21], respectively. Bateman [22] derives two variational principles for isentropic conditions; a maximum principle defined in terms of the velocity potential and a minimum principle defined in terms of the stream function. Manwell [23] proposes a variational integral for flow with shocks but does not present numerical results. His approach is similar to that presented earlier by Greenspan and Jain [24] where a variational principle is extremized using finite differences. This variational principle is the same as that derived by Lush and Cherry [25], which is based on the maximum principle of Bateman, for steady conditions. In this regard, the proposed method for optimal incremental approximation will be applied to the problem studied by Greenspan and Jain [24].

5.1 The velocity potential equation

The equations governing steady, two-dimensional, isentropic, inviscid, compressible fluid flow past a fixed body are given by the continuity and momentum equations

$$\frac{\partial(\rho u)}{\partial x} + \frac{\partial(\rho v)}{\partial y} = 0 \tag{13}$$

$$u\frac{\partial u}{\partial x} + v\frac{\partial u}{\partial y} + \frac{1}{\rho}\frac{\partial p}{\partial x} = 0 \tag{14}$$

$$u\frac{\partial v}{\partial x} + v\frac{\partial v}{\partial y} + \frac{1}{\rho}\frac{\partial p}{\partial y} = 0 \ . \tag{15}$$

In these equations, u and v are the x and y cartesian velocity components, respectively, ρ is density, and p is pressure. The velocity vector is defined as the gradient of the velocity potential φ

$$\bar{u} = (u, v)^{\mathrm{T}} = \nabla\varphi = \left(\frac{\partial\varphi}{\partial x}, \frac{\partial\varphi}{\partial y}\right)^{\mathrm{T}} \ , \tag{16}$$

with $V^2 = u^2 + v^2$. The set of equations is completed by the equation of state for an ideal gas

$$p = a\rho^{\gamma} \ , \tag{17}$$

where a is a constant and γ is the ratio of specific heats. Equations (13) - (15) can be combined to yield the potential velocity equation

$$\left(c^2 - \left(\frac{\partial\varphi}{\partial x}\right)^2\right)\frac{\partial^2\varphi}{\partial x^2} - 2\frac{\partial\varphi}{\partial x}\frac{\partial\varphi}{\partial y}\frac{\partial^2\varphi}{\partial x\partial y} + \left(c^2 - \left(\frac{\partial\varphi}{\partial y}\right)^2\right)\frac{\partial^2\varphi}{\partial y^2}\ , \tag{18}$$

where $c^2 = dp/d\rho$ is the square of the local speed of sound. The associated boundary conditions are

$$\frac{\partial\varphi}{\partial n} = 0 \quad , \quad \text{on the body surface and} \tag{19}$$

$$\nabla\varphi = (V_\infty, 0)^{\mathrm{T}} = \text{constant} \quad , \quad \text{far from the body,} \tag{20}$$

where n is the direction normal to the body surface and V_∞ is the freestream velocity, which is recovered far from the body.

5.2 The variational integral

If the velocity potential φ is defined in terms of some unknown auxiliary function χ according to

$$\varphi = V_\infty x + V_\infty \chi \quad , \tag{21}$$

then the maximum principle [22, 25] is given by

$$E(\varphi) = \int_\Omega \left(p - p_\infty + V_\infty \rho_\infty \frac{\partial(V_\infty\chi)}{\partial x}\right) d\bar{x} + \oint_C \left(\rho\varphi\frac{\partial\varphi}{\partial n} - V_\infty^2 \rho_\infty \chi \frac{\partial\chi}{\partial n}\right) ds\ , \tag{22}$$

where the subscript ∞ denotes freestream conditions and C represents the closed body curve. According to the boundary condition, $V_\infty\chi$, and hence χ, must vanish far from the body. The body considered in this paper is a unit cylinder. In this regard, a transformation to polar coordinates is utilized to derive the final functional

$$E(\chi) = p_\infty \int_{\theta=0}^{2\pi}\int_{r=1}^{\infty}(F - 1 + \gamma M_\infty^2 H) r dr d\theta\ , \tag{23}$$

where

$$F = \left(1 - \frac{\gamma-1}{2}M_\infty^2\left(2\cos(\theta)\frac{\partial\chi}{\partial r} - 2\frac{\sin(\theta)}{r}\frac{\partial\chi}{\partial\theta} + \left(\frac{\partial\chi}{\partial r}\right)^2 + \frac{1}{r^2}\left(\frac{\partial\chi}{\partial\theta}\right)^2\right)\right)^{\frac{\gamma}{\gamma-1}} \tag{24}$$

and

$$H = \left(1 - \frac{1}{r^2}\right) \frac{\partial \chi}{\partial r} \cos(\theta) - \left(1 + \frac{1}{r^2}\right) \frac{\partial \chi}{\partial \theta} \frac{\sin(\theta)}{r} \ . \tag{25}$$

Here, M_∞ denotes the freestream Mach number given by

$$M_\infty = \frac{V_\infty}{c_\infty} \ , \tag{26}$$

where c_∞ is the freestream speed of sound. Finally, the boundary conditions are

$$\frac{\partial \chi}{\partial r} = -\cos(\theta) \quad \text{at} \quad r = 1 \quad \text{and} \tag{27}$$

$$\chi = 0 \quad \text{far from the body.} \tag{28}$$

5.3 Computational domain and boundary conditions

The variational principle of Equation (23) is defined over an infinite domain. However, for the computations it has been assumed that the radius spans from the body surface ($r = 1$) to a radius of 20. This assumption is more than justified considering the fact that typical numerical grids in airfoil flow analysis extend to approximately seven times the body length. In addition, the flow is symmetrical about $\theta = 0$, $\theta = \pi$, $\theta = \pi/2$, and $\theta = 3\pi/2$. In this regard, the computational domain can be restricted to the range $\pi/2 \leq \theta \leq \pi$. With respect to the assumptions, the variational integral to be numerically maximized is given by

$$\int_{\theta_1=\pi/2}^{\theta_2=\pi} \int_{r_1=1}^{r_2=20} (F - 1 + \gamma M_\infty^2 H) r dr d\theta \ . \tag{29}$$

Figure 6 depicts the physical (x-y-plane) and computational (r-θ-plane) domains. The points A,B,C, and D with coordinates (-20,0), (-1,0), (0,1), and (0,20), respectively, are mapped on the points A*, B*, C*, and D*, with $r - \theta$ coordinates (20,π), (1,π), (1,$\pi/2$), and (20,$\pi/2$), respectively. The presence of homogeneous Dirichlet boundary conditions on the lines $r = 20$ and $\theta = \pi/2$ facilitates the use of basis functions that vanish at the domain boundaries. The presence of Neumann boundary conditions on the lines $r = 1$ and $\theta = \pi$, requires the extension of the computational domain, as shown in Figure 6. The extended computational domain is described by the points a, b, c, and D^* in the r-θ plane.

The boundary conditions have to be adjusted for the modified computational domain. Specifically, the appropriate boundary conditions are

$$\chi_r = -\cos(\theta) \quad \text{at} \quad r = 1 \ , \tag{30}$$

$$\chi = 0 \quad \text{at} \quad r = 20 \quad \text{and} \quad \theta = \frac{\pi}{2} \ , \tag{31}$$

and

$$\chi_\theta = 0 \quad \text{at} \quad \theta = \pi \ , \tag{32}$$

where the subscripts denote partial integration.

The Neumann boundary conditions are naturally satisfied by the variational principle, as shown in Appendix B.

5.4 Numerical procedure

The proposed algorithm for optimal incremental approximation has been utilized to numerically approximate the extremal function $\chi(r, \theta)$ that maximizes the variational principle. Utilizing the bilinear product $\Phi(r, \theta) = \Phi(r)\Phi(\theta)$ for the representation of the two-dimensional basis function, the function $\chi(r, \theta)$ is approximated by the series expansion

$$\chi_N^a(r, \theta) = \sum_{j=1}^{N} c_j \Phi_j(r, \bar{p}_j^r)\Phi_j(\theta, \bar{p}_j^\theta) \ , \tag{33}$$

where the basis functions Φ_j are B_1-splines with parameters $\bar{p}_j^r = (r_M, \Delta r_l, \Delta r_r)_j^{\mathrm{T}}$ and $\bar{p}_j^\theta = (\theta_M, \Delta\theta_l, \Delta\theta_r)_j^{\mathrm{T}}$. The c_j are the associated expansion coefficients.

The function $\chi(r, \theta)$ appears only implicitly, in the form of its partial derivatives with respect to r and θ in the functional. They are accordingly approximated by

$$\chi_r \approx \frac{\partial \chi_N^a}{\partial r} = \sum_{j=1}^{N} c_j \frac{\partial \Phi_j(r, \bar{p}_j^r)}{\partial r} \Phi_j(\theta, \bar{p}_j^\theta) \tag{34}$$

$$\chi_\theta \approx \frac{\partial \chi_N^a}{\partial \theta} = \sum_{j=1}^{N} c_j \Phi_j(r, \bar{p}_j^r) \frac{\partial \Phi_j(\theta, \bar{p}_j^\theta)}{\partial \theta} \ . \tag{35}$$

These approximations are introduced into the variational integral to be maximized at each step of the algorithm and PDS is employed to determine the optimal parameters and expansion coefficient.

Due to the high complexity and nonlinearity of the functional, the optimization problem cannot be decomposed into lower-dimensional problems; all seven optimization variables, represented by the vector $\bar{p}_j = (r_M, \Delta r_l, \Delta r_r, \theta_M, \Delta\theta_l, \Delta\theta_r, c)_j^{\mathrm{T}}$, are computed in one step by solving a seven-dimensional highly nonlinear optimization problem with the help of PDS. To enhance computational efficiency in the absence of simplification and decomposition possibilities, the scaling option of PDS was applied to the optimization variables. The components of the initial guess vector for each step of the algorithm were the following: r_M was positioned close to the cylinder surface, while Δr_l and Δr_r were chosen so that $\Phi(r)$ covers the computational domain in the r-direction; θ_M was positioned in the middle of the domain (with respect to the θ-direction), while $\Delta\theta_l$ and $\Delta\theta_r$ were also chosen so that $\Phi(\theta)$ covers the computational domain in the θ-direction. Finally, the initial guess for the coefficient c was set equal to zero so that the functional value achieved in the previous step of the algorithm will be the initial value in the next step. In this manner, it is guaranteed that the functional value will be strictly monotonically improved with each iteration of the proposed algorithm.

5.5 Numerical results

Numerical results are presented for transonic flow of air about a unit cylinder and compared to results presented by Greenspan and Jain in reference [24]. The following flow properties are estimated after solving for the function χ:

1. The nondimensionalized speed of the fluid
$$\left(\frac{V}{V_\infty}\right)^2 = 1 + 2\cos(\theta)\chi_r - 2\frac{\sin(\theta)}{r}\chi_\theta + (\chi_r)^2 + \frac{1}{r^2}(\chi_\theta)^2 , \tag{36}$$
2. the nondimensionalized local speed of sound
$$\left(\frac{c}{V_\infty}\right)^2 = \frac{1}{M_\infty^2} + \frac{1}{2}(\gamma - 1)\left(1 - \left(\frac{V}{V_\infty}\right)^2\right) , \tag{37}$$
3. the nondimensionalized pressure
$$\frac{p}{p_\infty} = \left(1 + \frac{1}{2}(\gamma - 1)M_\infty^2\left(1 - \left(\frac{V}{V_\infty}\right)^2\right)\right)^{\frac{\gamma}{\gamma-1}} , \tag{38}$$

4. the pressure coefficient

$$C_p = \frac{\frac{p}{p_\infty} - 1}{\frac{1}{2}\gamma M_\infty^2} \ , \tag{39}$$

5. the nondimensionalized density,

$$\frac{\rho}{\rho_\infty} = \left(\frac{p}{p_\infty}\right)^{\frac{1}{\gamma}} \ , \tag{40}$$

where $\gamma = 1.405$. Since the auxiliary function $\chi(\theta, r)$ is approximated by piecewise linear splines, its partial derivatives χ_r and χ_θ, required for the representation of the above mentioned quantities, are approximated by piecewise constants. Therefore, the partial derivatives of χ in this paper have been smoothed by a cubic polynomial fit in the least-squares sense so that the results can be compared against those from references [24], [25] and [26].

Numerical test cases for freestream Mach numbers 0.4, 0.43, and 0.46 are presented in Figures 7 through 12 and are compared to those presented by Greenspan and Jain [24]. Greenspan and Jain reported results for many test cases, but their Newton-like algorithm failed to converge for freestream Mach numbers that were greater then 0.43. In their numerical test cases $\Delta\theta = 9°$ and $\Delta r = 0.1$, 0.15, and 0.2 were used, i.e. a finite difference grid was used with $11 \times 191 = 2101$, $11 \times 127 = 1397$, and $11 \times 96 = 1056$ nodes, respectively. Greenspan and Jain compared their results for $M_\infty = 0.4$ to those presented by Lush and Cherry and Imai in references [25] and [26], respectively.

The approximate function $\chi_N^a(r, \theta)$ is plotted over the computational domain in Figure 7 for $M_\infty = 0.4$ using 31 optimally selected basis functions and associated coefficients. This figure is also representative of $\chi_N^a(r, \theta)$ for $M_\infty = 0.43$ and 0.46. The function exhibits a steep gradient in the r-direction near the cylinder surface and so is expected to be sensitive to r. A satisfactory level of accuracy is shown in Figure 8 for various radii, considering the sensitivity to r and the low number of optimal basis functions used relative to a uniform grid.

Figures 9 and 10 show the approximation of $\chi_N(r, \theta)$ obtained for various radii for $M_\infty = 0.43$ and $M_\infty = 0.46$ using $N = 30$ and $N = 41$ optimal basis functions, respectively.

It can be concluded that the agreement is satisfactory compared to the results of Greenspan and Jain. Moreover, the proposed method did not fail for $M_\infty > 0.43$; the results presented complete the ones reported in references [26, 25], and [24].

Figure 11 shows the nondimensionalized fluid velocity and sonic speed on the cylinder surface for the three test cases. The agreement with previously reported results is satisfactory. It can be seen how the flow remains purely subsonic throughout the domain for $M_\infty = 0.4$, while the flow becomes transonic for $M_\infty = 0.43$ and $M_\infty = 0.46$. The pressure coefficient distribution on the cylinder surface for the three test cases are presented in Figure 12. Again, the agreement with the available data confirms the potential of the method.

5.6 Computational work

The amount of computational work that PDS required at each step of the proposed algorithm for optimal sequential approximation has been monitored and is presented in Table 2. Computational work is recorded in terms of the numbers of required PDS iterations, function and constraint evaluations. The strictly monotonically decreasing functional value is included. As can be concluded by inspection of Table 2, the amount of computational work does not exhibit extremely high fluctuations as the algorithm advances. As the number of optimal basis function increases and the maximum value of the functional is asymptotically approached, the amount of work necessary for the improvement of the approximation is approximately the same.

6 Generalization aspects

The proposed method has been largely based on the utilization of variational principles. However, the derivation of variational principles for general problems is far from straightforward. Moreover, variational integrals may not always be associated with extremal functions. In this regard, an alternative is necessary.

The method of weighted residuals is a possible alternative. For example, minimizing $\langle R, R\rangle$, where R is the residual of a differential equation, corresponds to the well-known least-squares weighted residual method. However, the associated disadvantages include: 1) the necessity of developing techniques for the accommodation of the boundary conditions and the possible solution of a multi-objective optimization problem in the event that a given problem is governed by more than one differential equation, and 2) the nonuniqueness of the solution in nonlinear problems.

An alternative [1] to the least-squares method within the class of the method of weighted residuals can be found by utilizing the variational principle for the linear, self-adjoint problem $L[u(\bar{x})] = g(\bar{x})$, where $l\langle\cdot,\cdot\rangle$ is the bilinear symmetric differential form associated with the differential operator $L[\cdot]$, and $e_{N-1} = u(\bar{x}) - u^a_{N-1}(\bar{x})$,

$$E = \frac{1}{2} l\langle e_{N-1}, e_{N-1}\rangle - \frac{1}{2} l\langle u(\bar{x}), u(\bar{x})\rangle - \frac{1}{2}\frac{(l\langle e_{N-1}, \Phi_N(\bar{x})\rangle)^2}{l\langle \Phi_N(\bar{x}), \Phi_N(\bar{x})\rangle} \ . \tag{41}$$

The numerator of the last term of this equation can be rewritten as

$$(l\langle e_{N-1}, \Phi_N(\bar{x})\rangle)^2 = \langle R_{N-1}, \Phi_N(\bar{x})\rangle^2 \ , \tag{42}$$

where the differential equation residual R_{N-1} is equal to $g(\bar{x}) - L[u^a_{N-1}(\bar{x})]$. Therefore, the minimization of E in Equation (41) is equivalent to minimizing both $-\langle R_{N-1}, \Phi_N(\bar{x})\rangle^2$ and $l\langle \Phi_N, \Phi_N\rangle$. From a geometric perspective, this indicates that by maximizing $\langle R_{N-1}, \Phi_N\rangle^2$, the N-th basis function will be selected such that Φ_N is as parallel as possible to the previous equation residual R_{N-1}. For the sake of generalization, $\langle R_{N-1}, \Psi_N\rangle^2$ should be considered as the term to be maximized, where Ψ_N is a function of Φ_N.

The selection of the associated coefficient c_N according to another geometric consideration follows; the residual R_N is forced to be as orthogonal as possible to Ψ_N. In this regard, the objective function to be minimized is $\langle R_N, \Psi_N\rangle^2$, with c_N being the optimization variable. The equivalence of this technique to the Petrov-Galerkin method of weighted residuals is apparent. In fact, for linear problems the coefficient can be readily calculated by the Galerkin relation $\langle R_N, \Psi_N\rangle = 0$ rather than minimizing $\langle R_N, \Psi_N\rangle^2$.

7 Conclusions

A method of optimal incremental approximation for the solution of differential equations, formulated and proposed in reference [1], was applied to linear nonself-adjoint and nonlinear problems.

The proposed algorithm requires the solution of a nonlinear optimization problem at each step. Variational principles, succinctly and concisely representing differential equations and associated boundary conditions, are utilized to define the objective function(al). In this manner, the well-posed formulation of the optimization problem is guaranteed.

The proposed method is adaptive in nature although a grid is neither built nor adapted in the traditional sense. The computational overhead of the a-posteriori error estimation and adaptive process, present in traditional adaptive and multigrid techniques, is avoided; the "grid", defined by the location of the optimally selected basis functions, evolves with the solution. Moreover, complicated data structures are not required, since systems of equations are neither assembled nor solved, and numerical stability issues are limited to the nonlinear optimization process. The algorithm can be initialized with an empty set of basis functions and can utilize a broad class of functions.

It has been shown that the proposed method can be successfully applied to linear nonself-adjoint, and nonlinear problems associated with general boundary conditions. Accurate results and satisfactory convergence rates have been obtained. Specifically, the accuracy level of the numerical results presented is satisfactory considering the relatively low number and order of the optimal basis functions used in the solution representation. Moreover, the proposed method did not face the difficulties that traditional methods did in some applications. In addition, the proposed method fully exploits its adaptive nature in problems whose solutions exhibit large gradients.

Computational cost is reduced while efficiency is enhanced by the solution of the low-dimensional optimization problems by the parallel direct search (PDS) technique which features concurrent function evaluations. Readily parameterized low-order functions, and their bilinear products, have been used to ensure simplicity and computational efficiency. The computational work required by PDS for the solution of the nonlinear optimization problem, does not increase as the algorithm advances; the number of required PDS iterations, and function and constraint evaluations do not fluctuate dramatically.

The proposed method has been largely based on the utilization of natural and contrived variational principles. However, alternative formulations of optimization problems have been proposed for the determination of the optimal basis functions and the associated coefficients in problems where variational principles are not available.

Future research work could be focused on the extension of the method to three-dimensional and/or unsteady problems including irregular boundaries.

Acknowledgments

Access to the computing facilities of the Center for Research on Parallel Computation (CRPC) at Rice University, and the assistance of David Serafini with the optimal utilization of the PDS software are greatly appreciated. This work was supported under NASA grant # CRA2-35504 and ONR grant # N00014-95-1-0741.

REFERENCES

[1] A.J. Meade, Jr., M. Kokkolaras, and B.A. Zeldin. "Sequential function approximation for the solution of differential equations". *Communications in Numerical Methods in Engineering*, 13:977–986, 1997.

[2] P.S. Jensen. "Advances in computer methods for partial differential methods". In R. Vivhnevestjy, editor, *AICA Symposium*, pages 80–85, Lehigh University, 1975.

[3] E.R. Oliveira. "Optimization of finite element solutions". In *Proc. Third Conf. Matrix Methods in Struct. Mech.*, Ohio, 1971. Air Force Flight Dynamics Laboratory, Wright-Patterson AFB. AFFDL TR 71-160.

[4] C.A. Felippa. "Optimization of finite element grids by direct energy search". *Appl. Math. Modelling*, 1:93–96, 1976.

[5] C.A. Felippa. "Numerical experiments in finite element grid optimization by direct energy search". *Appl. Math. Modelling*, 1:239–244, 1977.

[6] L. Demkowicz and J.T. Oden. "On a mesh optimization method based on a minimization of interpolation error". *Int. J. Engng. Sci.*, 24(1):55–68, 1986.

[7] A.R. Diaz, N. Kikuchi, and J.E. Taylor. "A method of grid optimization for finite element methods". *Computer Methods in Applied Mechanics and Engineering*, 41:29–45, 1983.

[8] A.R. Diaz, N. Kikuchi, and J.E. Taylor. "Optimal design formulations for finite element grid adaptation". In V. Komokov, editor, *Lecture Notes in Mathematics: Sensitivity of Functionals with Applications in Engineering Science*. Springer Verlag, Berlin, 1984.

[9] J.T. Oden. "Adaptive methods in computational fluid dynamics". In T.J. Chung, editor, *Finite Elements in Fluids*. Hemisphere Publ. Corp., 1975.

[10] L.K. Jones. "Constructive approximations for neural networks by sigmoidal functions". *Proceedings of the IEEE*, 78(10):1586–1589, 1990.

[11] L.K. Jones. "A simple lemma on greedy approximation in Hilbert space and convergence rates for projection pursuit regression and neural network training". *The Annals of Statistics*, 20(1):608–613, 1992.

[12] A.R. Barron. "Universal approximation bounds for superpositions of a sigmoidal function". *IEEE Transactions on Information Theory*, 39(3):930–945, 1993.

[13] J.E. Dennis, Jr. and V. Torczon. "Direct search methods on parallel machines". *SIAM Journal of Optimization*, 1(4):448–474, November 1991.

[14] C.A.J. Fletcher. *Computational Techniques for Fluid Dynamics*, volume 1. Springer Verlag, 1988. Pages 293-299.

[15] O.C. Zienkiewicz and R.L. Taylor. *The Finite Element Method*. McGraw-Hill, 1989. Pages 240-242.

[16] A.J. Davies. *The Finite Element Method, a First Approach*. Clarendon Press, 1980. Pages 54-55.

[17] J.T. Oden. "A general theory of finite elements - II Applications". *Int. J. Num. Meth. Engng.*, 1:247–259, 1969.

[18] D. Greenspan. "On approximating extremals of functionals - I, The method and examples for boundary value problems". *Bull. Int. Comp. Centre*, 4(2):99–120, April-June 1965. University of Rome.

[19] D. Greenspan. "On approximating extremals of functionals - II, Theory and generalizations related to boundary value problems for nonlinear differential equations". *Int. J. Engng Sci.*, 5:571–588, 1967.

[20] R.J. Prozan. "A variational principle for compressible fluid mechanics - Discussion of the one-dimensional theory". Technical Report 3526, NASA, April 1982.

[21] R.J. Prozan. "A variational principle for compressible fluid mechanics - Discussion of the multi-dimensional theory". Technical Report 3614, NASA, 1982.

[22] H. Bateman. "Irrotational motion of a compressible inviscid fluid". *Proc. Nat. Acad. Sci*, 16:816–825, 1930.

[23] A.R. Manwell. "A variational principle for steady homenergic compressible flow with finite shocks". *Wave Motion*, 2(1):83–95, 1980.

[24] D. Greenspan and P.C. Jain. "Application of a method for approximating extremals of functionals to compressible flow". *Mathematical Analysis and Applications*, 18(1):85–111, April 1967.

[25] P.E. Lush and T.M. Cherry. "The variational method in hydrodynamics". *J. Mech. Appl. Math.*, 9:6–21, 1956.

[26] I. Iami. "On the flow of a compressible fluid past a circular cylinder". In *Proc. Phys. - Math. Soc. Japan*, pages 180–193, 1941. Ser. 3, volume 23.

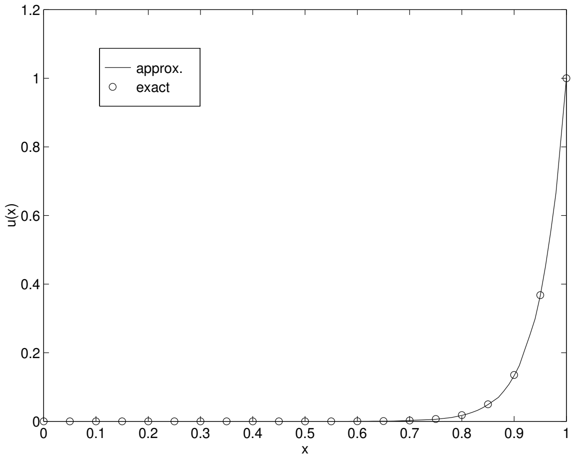

Figure 1: One-dimensional convection-diffusion; exact and approximate solutions using 14 optimal basis functions.

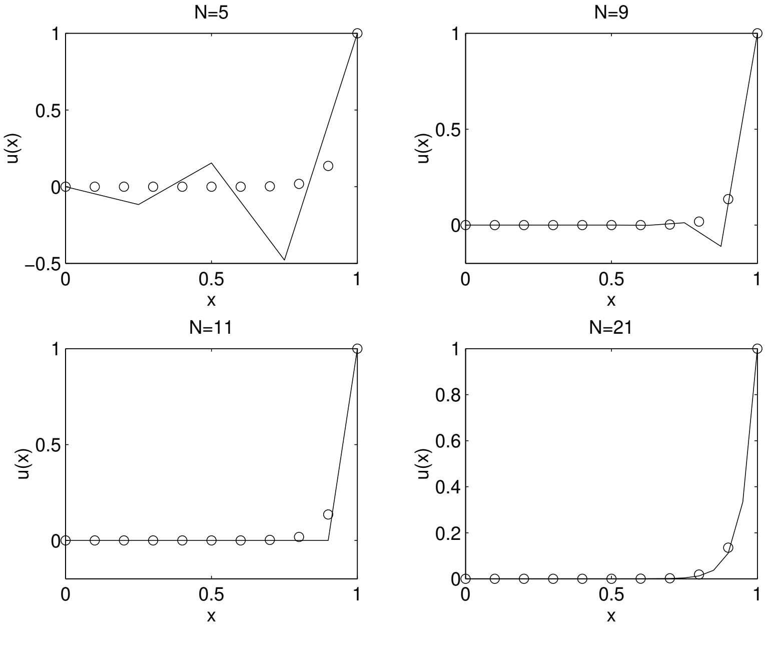

Figure 2: One-dimensional convection-diffusion; the evolution of the solution with increasing number of functions using the finite element method on a uniform grid with linear Lagrangian shape functions.

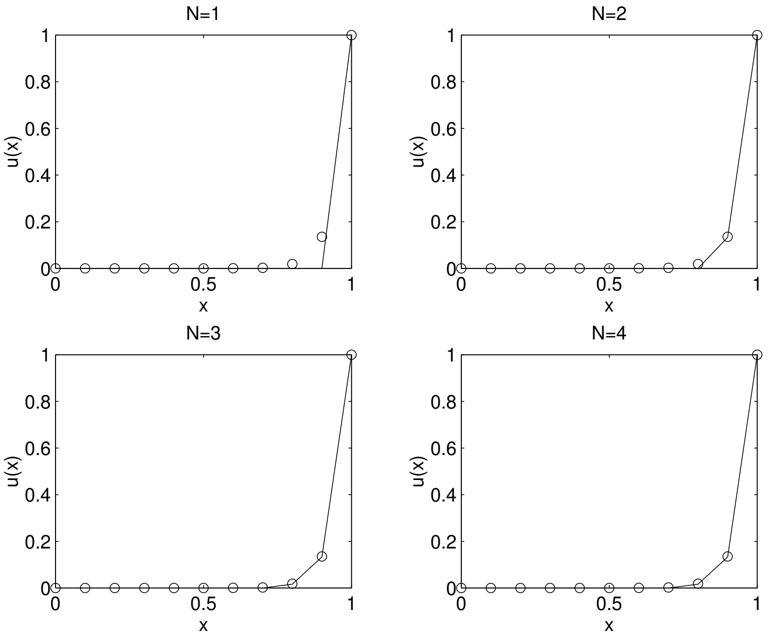

Figure 3: One-dimensional convection-diffusion; the evolution of the solution with increasing number of functions using the proposed method for optimal incremental approximation.

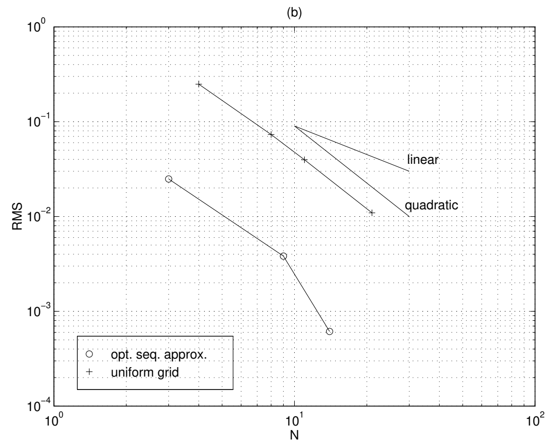

Figure 4: One-dimensional convection-diffusion; convergence rates comparison.

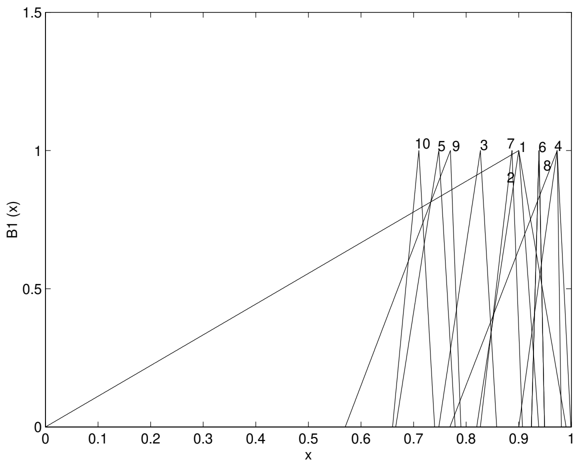

Figure 5: One-dimensional convection-diffusion; distribution of the first 10 optimally selected basis functions.

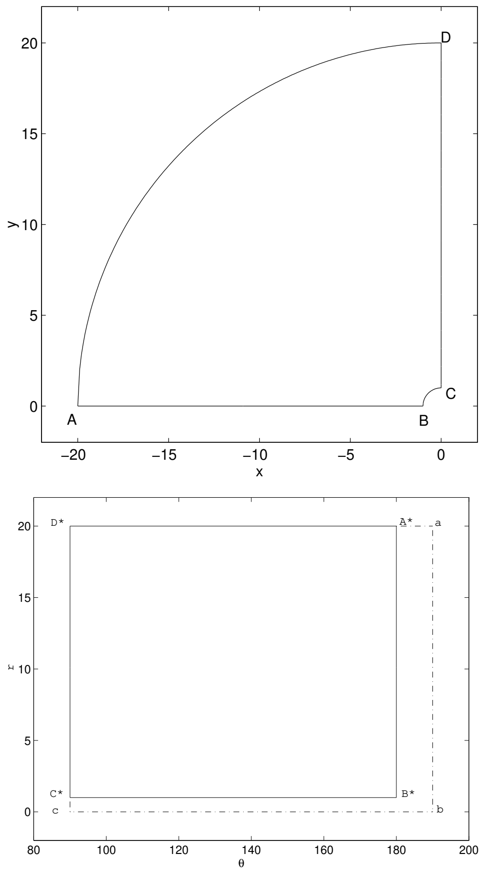

Figure 6: Two-dimensional, compressible, inviscid flow; the physical (x-y-plane) and computational (r-θ-plane) domains, top and bottom, respectively.

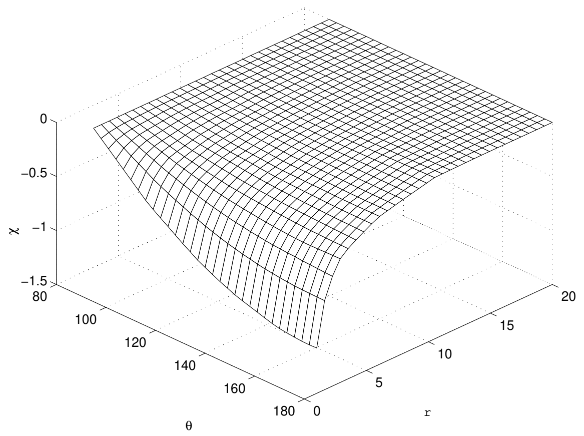

Figure 7: Two-dimensional, compressible, inviscid flow; the approximate velocity potential auxiliary function $\chi(r, \theta)$ for $M_\infty = 0.4$ using 31 optimal basis functions.

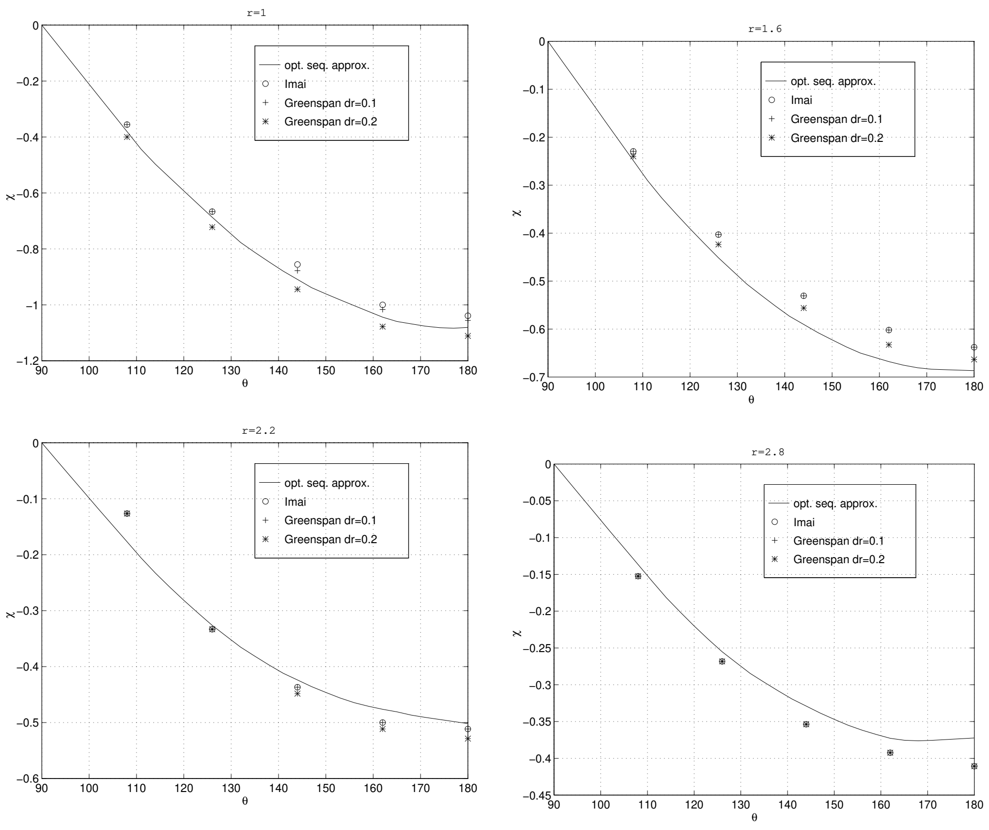

Figure 8: Two-dimensional, compressible, inviscid flow; the approximate velocity potential auxiliary function at $r = 1$, 1.6, 2.2 and 2.8 for $M_\infty = 0.40$ using 31 optimal basis functions.

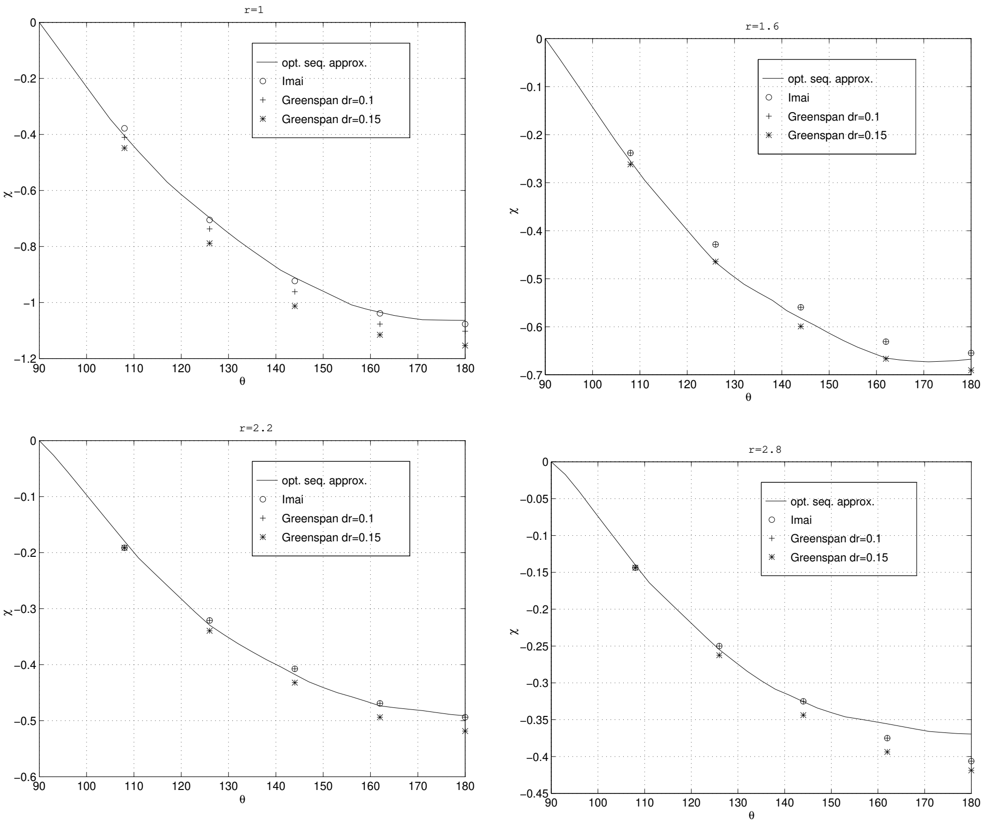

Figure 9: Two-dimensional, compressible, inviscid flow; the approximate velocity potential auxiliary function at $r = 1$, 1.6, 2.2 and 2.8 for $M_\infty = 0.43$ using 30 optimal basis functions.

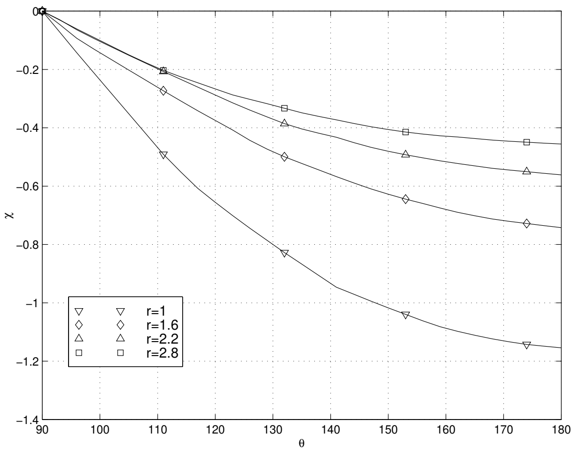

Figure 10: Two-dimensional, compressible, inviscid flow; the approximate velocity potential auxiliary function at $r = 1$, 1.6, 2.2 and 2.8 for $M_\infty = 0.46$ using 41 optimal basis functions.

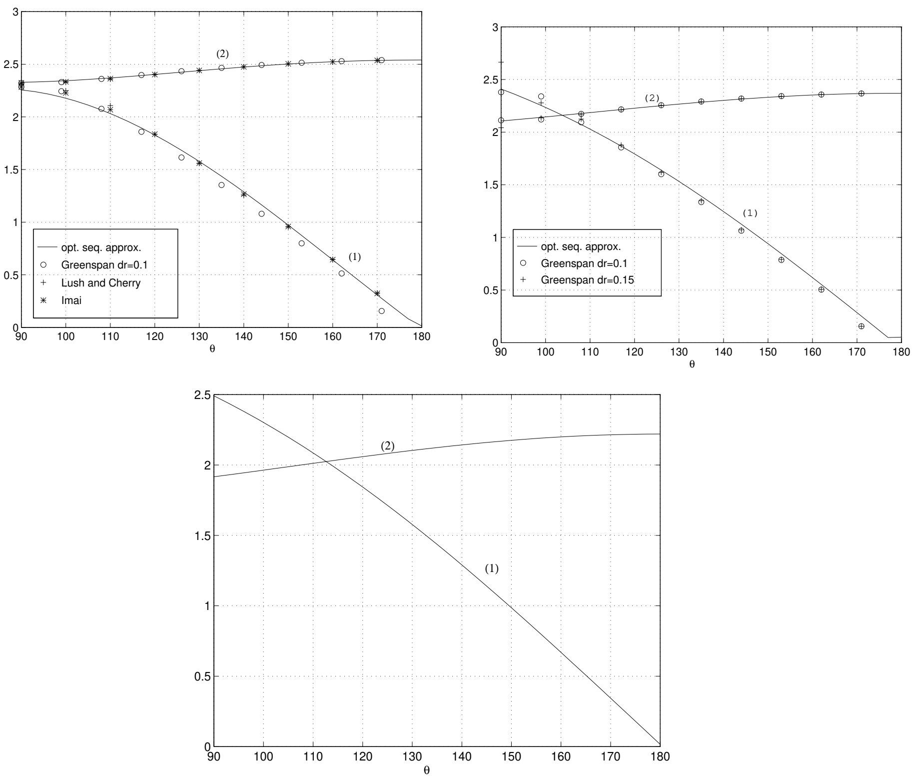

Figure 11: Two-dimensional, compressible, inviscid flow; (curve 1) nondimensionalized fluid velocity and (curve 2) sonic speed on the cylinder surface for (top left) $M_\infty = 0.4$, (top right) $M_\infty = 0.43$, and (bottom) $M_\infty = 0.46$.

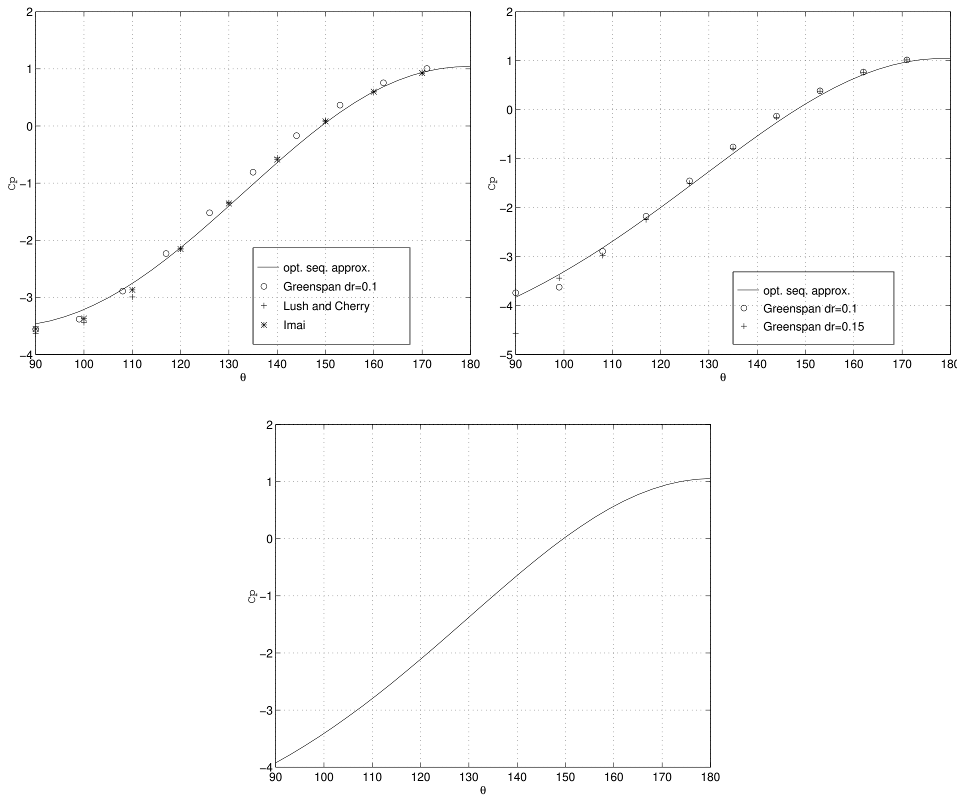

Figure 12: Two-dimensional, compressible, inviscid flow; pressure coefficients distribution on the cylinder surface for (top left) $M_\infty = 0.4$, (top right) $M_\infty = 0.43$, and (bottom) $M_\infty = 0.46$.

Table 1: Amount of computational work required by PDS for the linear convection-diffusion problem.

Algorithm step	# of PDS iterations	Total # of function eval.	Total # of constraint eval.
	$d = 100$	$tol = 10^{-6}$	
1	24	836	2272
8	18	1493	1536
16	15	1307	1365
24	16	1168	1335
	$d = 1000$	$tol = 10^{-4}$	
1	7	916	5344
8	11	5721	6683
16	12	6970	8719
24	10	7401	8475

Table 2: Amount of computational work required by PDS for the two-dimensional, compressible, inviscid flow problem using $d = 1120$ and $tol = 10^{-4}$.

Algorithm step	# of PDS iterations	Total # of function eval.	Total # of constraint eval.	Functional value
		$M = 0.4$		
1	21	6337	17202	0.053511
10	16	11464	12155	0.093902
20	42	33811	41611	0.095980
30	17	13711	15000	0.096385
		$M = 0.43$		
1	17	8014	12655	0.069409
10	15	7941	13806	0.106047
20	22	20452	21232	0.111336
30	24	19443	24323	0.113558
		$M = 0.46$		
1	17	7543	12654	0.080411
10	31	23691	27128	0.128511
20	44	28435	39596	0.143601
30	24	23453	23643	0.149425
40	37	36678	38842	0.150619

Appendix A

If $L[\cdot] = -\alpha \frac{d^2 \cdot}{dx^2} + \beta \frac{d \cdot}{dx}$, then $L'[\cdot] = P(x) L[\cdot]$ is self-adjoint if and only if for any two arbitrary functions z and w the relation

$$\int_a^b w L'[z] dx - \int_a^b z L'[w] dx = \int_a^b w P L[z] dx - \int_a^b z P L[w] dx =$$

$$\int_a^b w P \left(-\alpha \frac{d^2 z}{dx^2} + \beta \frac{dz}{dx} \right) dx - \int_a^b z P \left(-\alpha \frac{d^2 w}{dx^2} + \beta \frac{dw}{dx} \right) dx \tag{43}$$

is a function of the boundary terms that arise from integration by parts only. Integration by parts yields

$$\left[\int_a^b \left(\frac{d(wP\alpha)}{dx} \frac{dz}{dx} + wP\beta \frac{dz}{dx} \right) dx - (\text{B.T.})_1 \right] - \left[\int_a^b \left(\frac{d(zP\alpha)}{dx} \frac{dw}{dx} + zP\beta \frac{dw}{dx} \right) dx - (\text{B.T.})_2 \right] =$$

$$\int_a^b w \frac{d(P\alpha)}{dx} \frac{dz}{dx} dx + \int_a^b wP\beta \frac{dz}{dx} dx - (\text{B.T.})_1 - \int_a^b z \frac{d(P\alpha)}{dx} \frac{dw}{dx} dx - \int_a^b zP\beta \frac{dw}{dx} + (\text{B.T.})_2 =$$

$$\int_a^b w \frac{dz}{dx} \left(P\beta + \alpha \frac{dP}{dx} \right) dx - (\text{B.T.})_1 \quad - \int_a^b z \frac{dw}{dx} \left(P\beta + \alpha \frac{dP}{dx} \right) dx + (\text{B.T.})_2 \ , \tag{44}$$

where $(\text{B.T.})_1$ and $(\text{B.T.})_2$ denote the boundary terms. By examining Equation (44), it is obvious that, the necessary and sufficient condition for L' to be self-adjoint is

$$P\beta + \alpha \frac{dP}{dx} = 0 \ , \tag{45}$$

which yields after integration

$$P(x) = e^{-\frac{\beta}{\alpha} x} \ . \tag{46}$$

Appendix B

Assuming that the homogeneous Dirichlet boundary conditions are satisfied by the trial functions, the variation of $E(\chi)$ with respect to a variation in χ, defined as

$$\Xi = \chi + \epsilon \eta \tag{47}$$

with

$$\Xi_r = \chi_r + \epsilon \eta_r \quad \text{and} \quad \Xi_\theta = \chi_\theta + \epsilon \eta_\theta \ , \tag{48}$$

is given by

$$\left[\frac{\partial E}{\partial \epsilon}\right]_{\epsilon=0} = \int\int \left[\frac{\partial (Fr)}{\partial \epsilon}\right]_{\epsilon=0} drd\theta + \int\int \left[\frac{\partial (\gamma M^2 Hr)}{\partial \epsilon}\right]_{\epsilon=0} drd\theta \tag{49}$$

and must vanish, for E to be extremized.

In this regard, and by noting that

$$F = F(r, \theta, \chi_r, \chi_\theta) \ , \quad H = H(r, \theta, \chi_r, \chi_\theta) \ ,$$

$$r \neq r(\epsilon) \ , \text{and} \quad \theta \neq \theta(\epsilon) \ ,$$

it can be found that

$$\left[\frac{\partial (Fr)}{\partial \epsilon}\right]_{\epsilon=0} = \left[\frac{\partial (Fr)}{\partial \Xi_r}\frac{\partial \Xi_r}{\partial \epsilon}\right]_{\epsilon=0} + \left[\frac{\partial (Fr)}{\partial \Xi_\theta}\frac{\partial \Xi_\theta}{\partial \epsilon}\right]_{\epsilon=0} \tag{50}$$

and

$$\left[\frac{\partial (\gamma M^2 Hr)}{\partial \epsilon}\right]_{\epsilon=0} = \left[\frac{\partial (\gamma M^2 Hr)}{\partial \Xi_r}\frac{\partial \Xi_r}{\partial \epsilon}\right]_{\epsilon=0} + \left[\frac{\partial (\gamma M^2 Hr)}{\partial \Xi_\theta}\frac{\partial \Xi_\theta}{\partial \epsilon}\right]_{\epsilon=0} \ , \tag{51}$$

where

$$\frac{\partial \Xi_r}{\partial \epsilon} = \eta_r \quad \text{and} \quad \frac{\partial \Xi_\theta}{\partial \epsilon} = \eta_\theta \tag{52}$$

and

$$\left[\frac{\partial (Fr)}{\partial \Xi_r}\right]_{\epsilon=0} = -G^{\frac{1}{\gamma-1}}\gamma r M^2(\cos\theta + \chi_r) \equiv P \tag{53}$$

$$\left[\frac{\partial (Fr)}{\partial \Xi_\theta}\right]_{\epsilon=0} = -G^{\frac{1}{\gamma-1}}\gamma M^2(\frac{1}{r}\chi_\theta - \sin\theta) \equiv Q \tag{54}$$

$$\left[\frac{\partial (\gamma M^2 Hr)}{\partial \Xi_r}\right]_{\epsilon=0} = \gamma M^2(r - \frac{1}{r})\cos\theta \equiv R \tag{55}$$

$$\left[\frac{\partial (\gamma M^2 Hr)}{\partial \Xi_\theta}\right]_{\epsilon=0} = -\gamma M^2(1 + \frac{1}{r^2})\sin\theta \equiv S \ , \tag{56}$$

where

$$G = 1 - \frac{1}{2}(\gamma - 1)M^2(2\cos\theta\chi_r - 2\frac{1}{r}\sin\theta\chi_\theta + \chi_r^2 + \frac{1}{r^2}\chi_\theta^2) \ . \tag{57}$$

Substituting Equations (50)-(56) into Equation (49) yields

$$E = \int\int (P\eta_r + Q\eta_\theta)drd\theta + \int\int (R\eta_r + S\eta_\theta)drd\theta \ . \tag{58}$$

Integrating by parts the first terms of each integral with respect to r and the second terms of each integral with respect to θ yields

$$E = -\int\int \frac{\partial P}{\partial r}\eta dr d\theta - \int\int \frac{\partial Q}{\partial \theta}\eta dr d\theta + \int [P\eta]_{r_1}^{r_2} d\theta + \int [Q\eta]_{\theta_1}^{\theta_2} dr -$$
$$\int\int \frac{\partial R}{\partial r}\eta dr d\theta - \int\int \frac{\partial S}{\partial \theta}\eta dr d\theta + \int [R\eta]_{r_1}^{r_2} d\theta + \int [S\eta]_{\theta_1}^{\theta_2} dr \ . \tag{59}$$

But

$$\frac{\partial R}{\partial r} = -\frac{\partial S}{\partial \theta} \ , \tag{60}$$

and η is zero on $r = r_2$ and $\theta = \theta_1$ (due to the homogeneous Dirichlet boundary conditions on these boundaries) and so the functional variation reads

$$E = -\int\int \left(\frac{\partial P}{\partial r} + \frac{\partial Q}{\partial \theta}\right) \eta dr d\theta - \int [P\eta]_{r_1} d\theta + \int [Q\eta]_{\theta_2} dr - \int [R\eta]_{r_1} d\theta + \int [S\eta]_{\theta_2} dr \ . \tag{61}$$

In addition, $[R]_{r_1} = 0$ and $[S]_{\theta_2} = 0$ and, therefore, the final functional variation is given by

$$E = -\int\int \left(\frac{\partial P}{\partial r} + \frac{\partial Q}{\partial \theta}\right) \eta dr d\theta - \int [P\eta]_{r_1} d\theta + \int [Q\eta]_{\theta_2} dr \ . \tag{62}$$

In order for E to vanish for arbitrary η, all the integrands must vanish, i.e.

$$\frac{\partial P}{\partial r} + \frac{\partial Q}{\partial \theta} = 0 \ , \tag{63}$$

$$[P]_{r_1} = 0 \ , \tag{64}$$

and

$$[Q]_{\theta_2} = 0 \ . \tag{65}$$

Equation (63) is the associated Euler-Lagrange equation of the functional, and Equations (64) and (65) are the Neumann boundary conditions on $r = r_1$ and $\theta = \theta_2$, respectively. Specifically, from Equation (64)

$$\left[-G^{\frac{1}{\gamma-1}}\gamma r M^2(\cos\theta + \chi_r)\right]_{r_1} = 0 \Longrightarrow$$
$$\left[G^{\frac{1}{\gamma-1}}\right]_{r_1} = 0 \quad \text{or} \quad [\cos\theta + \chi_r]_{r_1} = 0 \tag{66}$$

and from Equation (65)

$$\left[-G^{\frac{1}{\gamma-1}}\gamma M^2(\frac{1}{r}\chi_\theta - \sin\theta)\right]_{\theta_2} = 0 \Longrightarrow$$

$$\left[G^{\frac{1}{\gamma-1}}\right]_{\theta_2} = 0 \quad \text{or} \quad \left[\frac{1}{r}\chi_\theta\right]_{\theta_2} = 0 \ . \tag{67}$$

Since $G^{\frac{1}{\gamma-1}}$ represents the density of the fluid, and can therefore not be equal to zero, the Neumann boundary conditions are given by

$$\chi_r = -\cos\theta \quad \text{on} \quad r = r_1 \tag{68}$$

and

$$\chi_\theta = 0 \quad \text{on} \quad \theta = \theta_2 \ , \tag{69}$$

which are indeed the (homogeneous and nonhomogeneous) Neumann boundary conditions of the problem and are therefore naturally satisfied by the functional of Equation (23).